GDCh Research Article Angewandte International Edition Chemie www.angewandte.org

How to cite: *Angew. Chem. Int. Ed.* **2025**, *64*, e202515531
doi.org/10.1002/anie.202515531

Analytical Chemistry

Chiral Discrimination of all Proteinogenic Amino Acid Enantiomers by Nanopore Sensing

Hanhan Zhang[+], *Kefan Wang*[+], *Xiao Zhou*[+], *Yifan Wang, Panke Zhang, Wenfei Li,* and Shuo Huang**

Abstract: D-amino acids, the stereoisomers of the more prevalent L-forms, are ubiquitously distributed across microorganisms, plants, and mammalian systems. Recent advances have uncovered their indispensable roles in biological processes, yet direct, single-molecule detection of D-amino acids has long been understudied. The simultaneous discrimination of all amino acid enantiomers remains a formidable analytical challenge. Here, we report a nickel-ion chelated hetero-octameric *Mycobacterium smegmatis* porin A (MspA) (MspA-NTA-Ni) nanopore sensor that achieves simultaneous identification of all 19 D-amino acids corresponding to proteinogenic L-isomers. By integrating supervised machine learning algorithms, this system demonstrated an overall recognition accuracy of 99.5%. The method was further validated in analyzing acid-hydrolyzed D-peptide products, yielding clear compositional profiles of amino acid enantiomers. Notably, the technology enables simultaneous sensing of all 39 amino acid enantiomers with an overall accuracy of 98.9%. This approach not only allows direct characterization of DL-amino acid mixtures but also provides a critical sensor component for nanopore-based exo-sequencing of D-peptides and D-proteins.

Introduction

Amino acid enantiomers arise from the tetrahedral configuration of the α-carbon atom, creating non-superimposable mirror images.[1] D-amino acids, long considered non-proteinogenic counterparts to their L-isomers, are now recognized as ubiquitously distributed in nature.[2] These include, but are not limited to, peptidoglycan components in Gram-positive bacterial cell walls[3] and bioactive peptides in antibiotics.[4–6] Their roles extend to mammalian systems, where D-serine[7] and D-aspartate[8] mediate critical neurotransmission and endocrine functions. Additionally, D-amino acids endow peptides with proteolytic resistance, making them promising candidates for therapeutic development and food preservation.[9] However, their identical molecular masses and physicochemical properties pose significant challenges for stereospecific analysis.[10]

Existing analytical methods for amino acid enantiomer discrimination include electrochemical fluorescence,[11] pre-column derivatization HPLC,[12,13] chiral stationary phase chromatography, NMR,[14,15] and capillary electrophoresis.[16] These well-established techniques are widely used and supported by mature instrumentation and standardized protocols. However, these techniques often require extensive sample preparation,[13] rely on complex or specialized instrumentation,[17] and may lack real-time monitoring capability or portability.

Nanopore sensing is an emerging single-molecule technique widely known for its use in nucleic acid sequencing.[18–20] Its success in nucleic acid sequencing has also stimulated various recent approaches aiming for nanopore protein sequencing.[21–26] Nanopore sensing of amino acids has been previously demonstrated by solid-state nanopores[27] and metal-ion modified biological nanopores.[24,28–31] A copper(II) modified α-hemolysin (α-HL) nanopore has previously demonstrated direct discrimination of amino acid enantiomers. However, restricted to a limited resolution, only 5 pairs of amino acid enantiomers were demonstrated.[28] Chiral peptides with amino acid differences can also be discriminated by aerolysin,[32] α-HL,[33] OmpF,[34] FraC and CytK[35] nanopores. However, sensing and discrimination of standalone amino acids was not reported by these works.

Previously, by installing a nickel ion-bound nitrilotriacetic acid (NTA-Ni) adapter to a hetero-octameric MspA,[18,24,31,36–38] simultaneous and unambiguous discrimination of all 20 proteinogenic L-amino acids and their representative post-translational modification were demonstrated.[24]

[*] H. Zhang[+], K. Wang[+], Y. Wang, Dr. P. Zhang, Prof. S. Huang
State Key Laboratory of Analytical Chemistry for Life Sciences, School of Chemistry and Chemical Engineering, Nanjing University, Nanjing 210023, China
E-mail: shuo.huang@nju.edu.cn

H. Zhang[+], K. Wang[+], Y. Wang, Prof. S. Huang
Chemistry and Biomedicine Innovation Center (ChemBIC), ChemBioMed Interdisciplinary Research Center, Nanjing University, Nanjing 210023, China

X. Zhou[+], Prof. W. Li
Collaborative Innovation Center of Advanced Microstructures, National Laboratory of Solid State Microstructure, Department of Physics, Nanjing University, Nanjing 210023, China
E-mail: wfli@nju.edu.cn

[+] These authors contributed equally to this work.

Additional supporting information can be found online in the Supporting Information section

This nickel ion-bound MspA nanopore (MspA-NTA-Ni) is, in principle, also suitable for sensing of all D-amino acids (Figure 1a), positioning it as a critical sensor component for potential "exo-sequencing"[39] applications of D-peptide or D-protein. Notwithstanding this potential, no nanopore sensor has yet been demonstrated to resolve all amino acid enantiomers simultaneously.

Results and Discussion

Sensing of D-amino Acids by MspA-NTA-Ni

Here, MspA-NTA-Ni is prepared (Figure S1) and used for D-amino acid sensing (Figure 1b). Given that glycine, the simplest proteinogenic amino acid, lacks an enantiomer, D-alanine was chosen as the model compound for the feasibility test (Figure 1c). Experimentally, the nanopore sensing device consists of two opposing chambers filled with a 1.5 M KCl buffer (1.5 M KCl, 10 mM CHES, pH 9.0). A pair of Ag/AgCl electrodes, electrically connected to a patch clamp amplifier, was inserted into each chamber, in contact with the buffer. Conventionally, the electrically grounded chamber is defined as the *cis* chamber, while its opposite compartment is defined as the *trans* chamber. After the insertion of a single MspA-NTA-Ni, measurements were conducted by continuously applying a +100 mV bias. The conductance features of MspA-NTA-Ni was also demonstrated (Figure S2 and Table S1). To enable simultaneous discrimination of proteinogenic amino acid enantiomers, the same conditions used for identifying 20 proteinogenic L-amino acids[24] were deliberately employed.

Immediately after adding D-alanine to the *cis* chamber to a final concentration of 2 mM, successive nanopore events, manifested as repetitive switching between I_0 and I_b, were observed (Figure 1c). However, this capacity could not be achieved when an MspA containing no NTA adapter or an MspA-NTA containing no Ni^{2+} was tested (Figure S3). Here, I_0 and I_b represent the current levels corresponding to the unbound and amino acid bound states of MspA-NTA-Ni, respectively. The frequency of these events increases as the final concentration of D-alanine added to the *cis* chamber was raised from 0.5 to 20 mM (Figure S4a–f), which confirmed that I_b was generated by the binding of the added D-alanine. Using D-alanine as a model compound, the ability of MspA-NTA-Ni to sense D-amino acids was effectively demonstrated.

To quantitatively characterize the sensing events, event parameters including open pore current (I_0), event current (I_b), blockage depth ($\Delta I = I_b - I_0$), noise amplitude (SD), event dwell time (t_{off}), inter-event duration (t_{on}), mean dwell time (τ_{off}) and mean inter-event duration (τ_{on}) are defined in Figure S5. For D-alanine, the reciprocal of the mean inter-event duration ($1/\tau_{on}$, $N = 3$) is proportional to the concentration of D-alanine. This finding is in line with a bimolecular model (Figure S4g and Table S2). In contrast, the reciprocal of the mean dwell time ($1/\tau_{off}$, $N = 3$) is independent of the D-alanine concentration (Figure S4h and Table S2), which is consistent with a unimolecular model. Based on three independent measurements conducted under the same conditions ($N = 3$), the event scatter plot of ΔI and SD derived from the D-alanine results exhibits a single and narrowly distributed population of events, indicating a high level of consistency and reproducibility of the events (Figure S6a).

To testify the generality of this method, all 19 D-amino acids were separately sensed (Figure 1d), according to results of which, each type of D-amino acid reports a unique event feature, which is desired for direct event identification (Figures 1d and S6–S15). Similar to that reported by L-amino acids,[24] when probed by MspA-NTA-Ni, all D-amino acids report positive-going events ($I_b > I_0$). Specifically, D-arginine and D-lysine, which are positively charged, report smaller I_b values. In contrast, D-aspartic acid and D-glutamic acid, which are negatively charged, report larger I_b.[24] By applying a +1 mV bias, which minimizes the contribution of the electrophoretic force, amino acid events were still detectable (Figure S16), suggesting that amino acids with different charges can spontaneously diffuse to the reactive adapter to trigger event generation. Moreover, amino acids with different charges can be simultaneously sensed at the same concentration, and there is no significant difference in the event counts (Figure S17).

Although most D-amino acids produce a single type of sensing event, D-histidine and D-proline could simultaneously report two types of events. This phenomenon may result from distinct binding configurations influenced by the imidazole side chain of D-histidine[40] and the cyclic structure of D-proline. For clarity, different types of D-histidine and D-proline events are respectively marked as type I and type II events.

To evaluate the consistency of the results, under the same conditions, all the above measurements were independently carried out ($N = 3$), and highly reproducible data were observed (Figures S6–S15). Corresponding core event parameters (ΔI, SD, etc.) are summarized in Table S3. By simultaneously considering ΔI and SD (Figure 1e), events produced by 19 D-amino acids and glycine can be well discriminated, though some event overlaps were still observed, as shown for events within the black box in Figure 1e. Of these, D-Ser, D-Ala, and Gly events overlap in the two-dimensional scatter plot of ΔI and SD (Figure S19b), but their event shapes are significantly different (Figure S19a) and can be distinguished when their *Spectral centroid* parameter is simultaneously considered (Figures S18, S19). Here, *Spectral centroid* represents the "center of gravity position" of the spectrum energy distribution of the signal and is the weighted average of the frequency components.[41] Generally, by the inclusion of the frequency domain parameter *Spectral centroid* (Figure S18), nanopore discrimination of all 19 D-amino acids has been well demonstrated by MspA-NTA-Ni (Figure 1f). However, after an extensive literature search, it was found that the simultaneous discrimination of all enantiomers of proteinogenic amino acids, which is crucial for exo-sequencing of D-peptides or D-proteins, has not been previously reported by any nanopore approach.

The higher analyte concentrations (0.5–20 mM) were intentionally selected to ensure rapid data collection. Notably, varying concentrations had no impact on event signatures (Figure S20). Detection of other representative amino acids

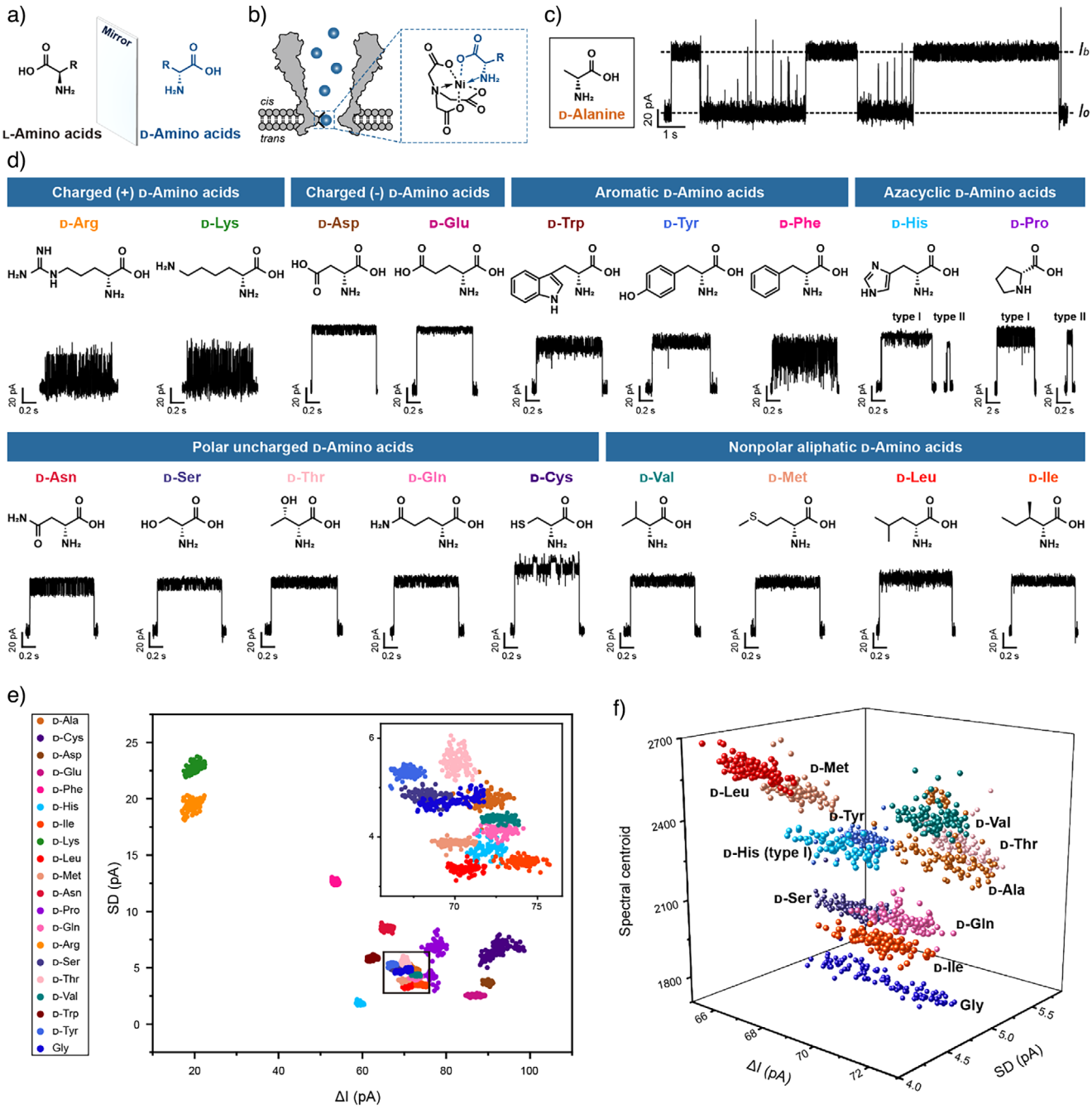

Figure 1. Discrimination of 19 D-amino acids and glycine using MspA-NTA-Ni. a) The structures of DL-amino acids. b) The molecular mechanism of D-amino acid sensing performed by MspA-NTA-Ni. c) A representative trace acquired with D-alanine using MspA-NTA-Ni. Here, I_0 represents the open pore current level of MspA-NTA-Ni. I_b represents the current level resulting from amino acid binding. d) Representative events acquired with different D-amino acids using MspA-NTA-Ni. D-His and D-Pro both produce two types of nanopore events, respectively defined as type I and type II. e) The event scatter plot of ΔI versus *SD* of events acquired with different D-amino acids and glycine. One hundred events acquired with each amino acid were used to generate the plot. To clarify the detail, the events inside the black box are further zoomed in and shown in the right corner. f) The 3D event scatter plot of ΔI, *SD* and *Spectral centroid* (Figure S18) generated by events acquired with D-Ala, D-His, D-Ile, D-Leu, D-Met, D-Gln, D-Ser, D-Thr, D-Val, D-Tyr, and Gly. All corresponding events are marked in the black box in 3e. All nanopore results demonstrated in c-f were measured as described in Methods. A +100 mV bias was continually applied. Different amino acids were separately added to *cis* with a final concentration of 0.5 mM (D-Cys, D-Asp, and D-Tyr), 1 mM (D-Ser, D-Gln, and D-Glu), 2 mM (D-Ala, D-Val, D-Met, D-Leu, D-Asn, D-Thr, D-Arg, D-Lys, D-Trp, D-Phe, and D-His), 4 mM (D-Ile), or 20 mM (D-Pro) (Figures S6–S15, Table S3).

at micromolar levels further validates the applicability of this method for low analyte concentrations (Figure S21). Going forward, extended measurement time and large nanopore arrays might be employed to further lower the detection limit. Additionally, the sensing specificity arises from specific interactions between the NTA-Ni adapter and the analyte. Thus, high analyte concentrations do not produce signals purely via mass action (Figure S22).

Identification of D-amino Acids by Machine Learning

To attain unbiased and automated event identification, a customized machine learning algorithm was developed (Methods). The entire machine learning process comprises three modules: dataset input, feature extraction, and model building. Specifically, a total of 6000 events, each separately obtained from different D-amino acids and glycine, were initially gathered to construct a dataset. Subsequently, this dataset was partitioned into a training set (accounting for 80% of the data) for model training and a testing set (20%) for model evaluation. Here, five time-domain features, including blockage depth (ΔI), noise amplitude (SD), dwell time (t_{off}), skewness ($skew$) and kurtosis ($kurt$)) of the blockage level of each event was extracted using a custom MATLAB code. Skewness quantifies the asymmetry of a distribution, while kurtosis characterizes the sharpness of its peak and heaviness of its tails (Figure S23). Furthermore, the frequency-domain features, including *Spectral centroid*, *Main frequency*, *Spectral energy* and *Spectral entropy*, were obtained via fast Fourier transform (FFT)[42] of the time-domain data (Methods). They respectively represent the position of the spectral centroid, the frequency point with the highest energy, the total energy of the spectrum, and the uniformity of the spectral energy distribution. Here, the inclusion of frequency-domain parameters, which capture event details not readily apparent in the time domain, provides a more comprehensive characterization of event features. When combined with the five widely employed time-domain features, this integrated feature set enhances discriminative capability and thereby boosts the accuracy of event identification.

To conduct comprehensive and accurate event analysis, a 9D feature matrix was constructed by integrating five time-domain and four frequency-domain features. Every event within this matrix was labeled according to the identity of the analyte that generated it. Subsequently, the feature matrix was imported into the Classification Learner toolbox of MATLAB for model training. Seven widely-used classifiers were evaluated, namely ensemble, SVM (Support Vector Machine), decision trees, naive Bayes, neural network, discriminant analysis, and KNN (k–Nearest Neighbor). To prevent overfitting, the performance of each model was assessed using 10-fold cross-validation. Among these classifiers, the derived cubic SVM model emerged as the top performer, achieving an impressive validation accuracy of 99.5% (Figure 2a and Table S6). In contrast, when only a 2D or 5D matrix of time-domain features was employed as the input dataset for training and validation, the validation accuracy decreased to 92.7% (Table S4), 98.3% (Table S5, Figure S24). Notably, for specific D-amino acids, the inclusion of frequency-domain parameters led to a substantial increase in their true positive rate (TPR). For instance, the TPR of D-Ala and D-Ser increased by 8.0% and 5.4% respectively (Figure S24). Furthermore, the feature importance of the optimized cubic SVM model is presented in Table S7, which shows that all parameters play crucial roles. This finding suggests that combining both time-domain and frequency-domain characteristics of events improves the discrimination of similar event signatures.

To assess the model training efficiency, the corresponding learning curve was generated (Figure S25). The confusion matrix generated by the cubic SVM model, as depicted in Figure 2b, reveals that all D-amino acid events have a minimum TPR of 98%, eight D-amino acids attain a 100% TPR, and the maximum false positive rate (FPR) is only 0.13% (Table S8). This trained cubic SVM model was further utilized for predicting unlabeled amino acid events obtained from a mixture of 19 D-amino acids. Representative traces are presented in Figures 2c–f, and all events were predicted and labeled using machine learning (Figures 2c–f and S26–S28). As an indicator of its performance, the corresponding event scatter plot of ΔI versus SD before and after event identification by machine learning is shown in Figure S29. In conclusion, with the assistance of the custom-developed machine learning algorithm, automated and rapid identification of all D-amino acids was achieved, even when they were measured as a heterogeneous mixture. Notably, the rigid conical pore lumen of MspA has provided highly consistent event signatures. Moreover, the NTA-Ni adapter is critical for generating distinctive event signatures, which collectively provide high-quality training data for machine learning model development.

To demonstrate concentration dependence (Methods), we selected three representative D-amino acids (D-Phe, D-Met, and D-Ser) for concentration-dependent assay. Notably, the event dwell time (τ_{off}) remained concentration-independent, while the event appearance frequency ($1/\tau_{on}$) showed a linear increase with analyte concentration (Figures S30–S32 and Tables S9–S11). D-amino acid concentrations in mixtures can also be quantified based on the calibrated event appearance frequency (Figure S33 and Table S12).

Analysis of D-amino Acids in Acid Hydrolysis Products of D-peptide

D-amino acids are ubiquitously distributed across diverse organisms, serving as key components in short peptides, peptidoglycans,[43] antibiotics,[44] toxins, and venoms.[45] However, despite extensive research, no naturally occurring proteins composed entirely of D-amino acids have been identified to date. Instead, D-peptides can be synthesized via well-established solid-phase peptide synthesis (SPPS) techniques.[46] Accumulating evidence suggests that mirror-image peptides and proteins have garnered significant attention as promising therapeutic and enzymatic tools due to their resistance to natural-chirality protease digestion and

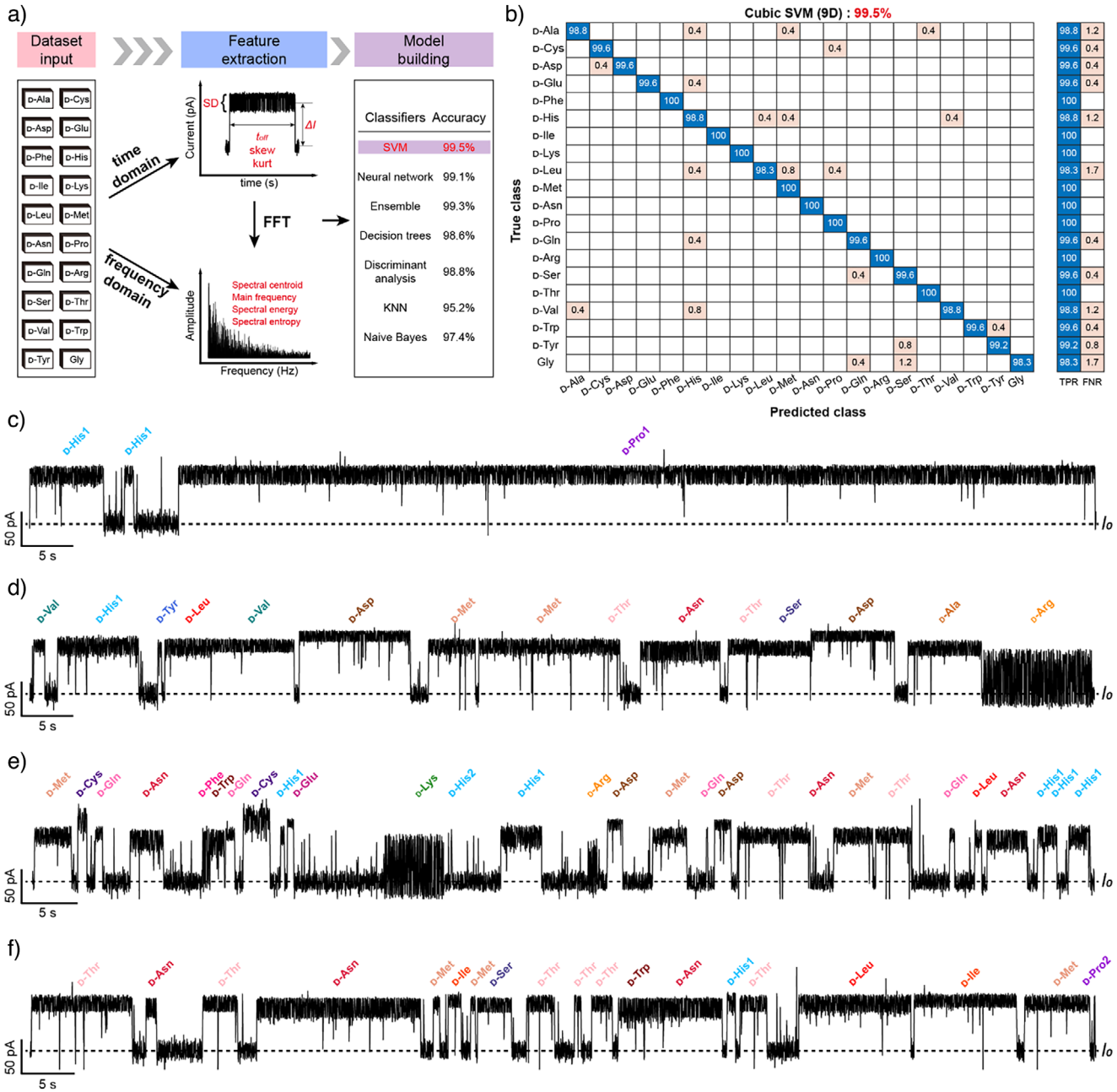

Figure 2. Identification of D-amino acids by machine learning. a) The workflow of machine learning. Briefly, sensing events separately acquired with 19 D-amino acids and glycine were collected to form a dataset. Each class is composed of 300 events. From each event, different features were extracted to form a feature matrix. Here, five parameters in the time-domain (ΔI, *SD*, t_{off}, skewness (*skew*) and kurtosis (*kurt*)) and four parameters in the frequency-domain (*Spectral centroid*, *Main frequency*, *Spectral energy* and *Spectral entropy*) were extracted. Machine learning was performed with the Classification Learner toolbox of MATLAB. Seven classifiers were evaluated with 10-fold cross-validation to screen the best-performing model. For the nine-feature machine learning, the highest validation accuracy reaches 99.5%, achieved by the cubic SVM model (Table S6). b) The confusion matrix of the testing set generated by the cubic SVM model of nine-feature machine learning. TPR (true-positive rate) and FNR (false-negative rate) represent the correct or false classification of each true class, respectively. (c-f) Representative traces acquired during simultaneous sensing of all 19 D-amino acids. The measurements were performed as described in Methods. A bias of +100 mV was continually applied. All D-amino acids were simultaneously added to *cis*. The final concentration of D-Trp, D-Tyr, D-Phe, D-His, D-Cys, D-Arg was 0.1 mM. The final concentration of D-Ile, D-Glu, D-Ala was 1 mM. The final concentration of D-Pro was 5 mM. The concentration of all remaining D-amino acids was 0.5 mM. All events were automatically predicted and labeled by machine learning prediction results. The open pore current (I_0) is marked with a dashed line in c-f. Zoomed-in views of these traces are also shown in Figures S26–S28 to show more details.

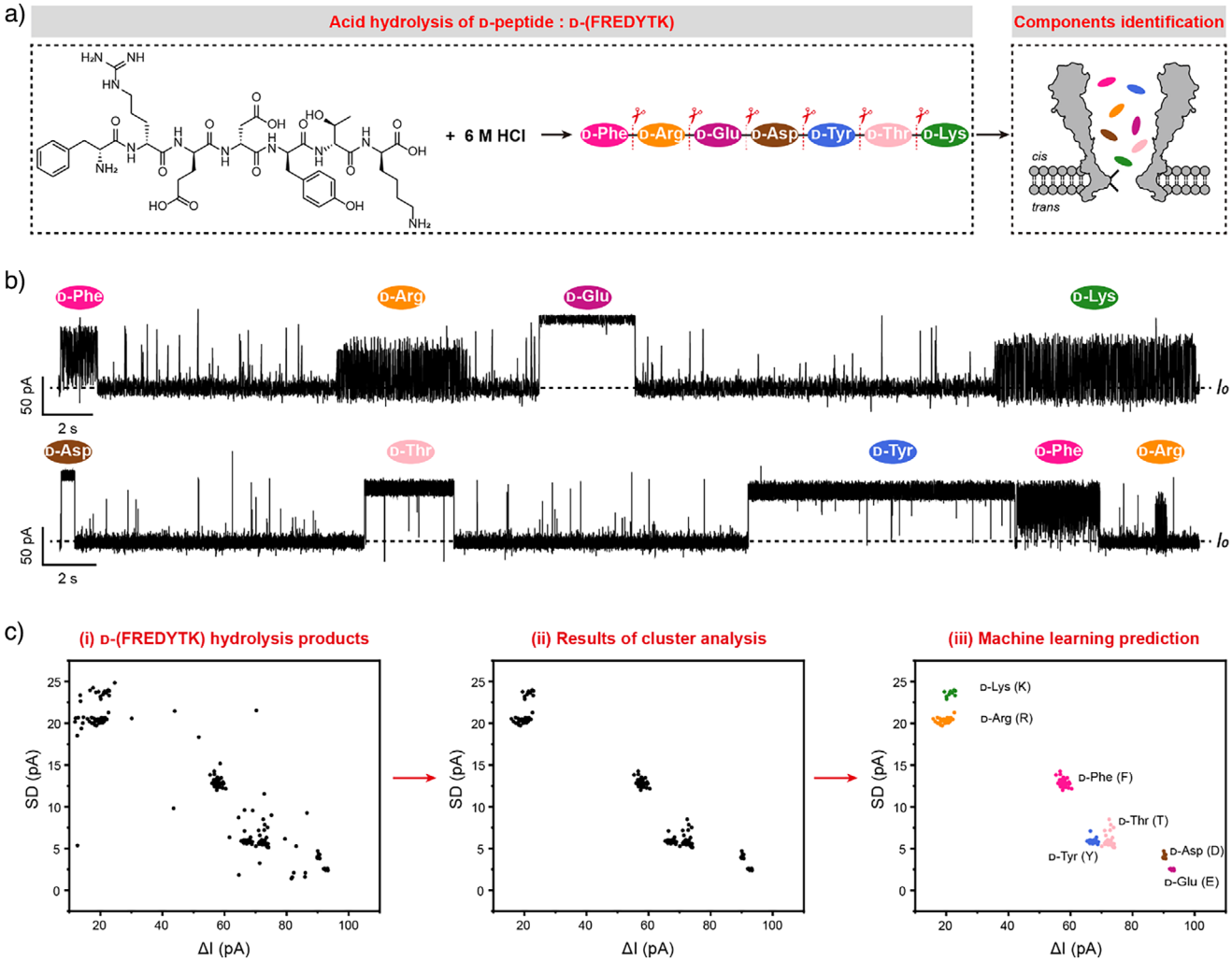

Figure 3. Identification of D-amino acids produced by acid hydrolysis of D-peptide. a) The schematic diagram of the identification of acid hydrolysis produced D-amino acids using MspA-NTA-Ni. Prior to the measurement, 6 M HCl was used to hydrolyze the D-peptide (FREDYTK) to generate the D-amino acids (Methods), which were then identified by MspA-NTA-Ni, enabling analysis of the D-amino acid components of the original D-peptide. b) Representative traces acquired with the acid hydrolysis product of the D-peptide (FREDYTK). D-amino acids were identified by measurement and labeled by the corresponding results of machine learning. c) Noise reduction and event prediction. All data obtained from a 60 min continuous recording were used. Left: The raw scatter plot of ΔI versus SD of events acquired with acid hydrolysis product of D-(FREDYTK) (n = 241). Middle: The scatter plot of events however after noise reduction treatment performed by DBSCAN. The epsilon was set to 1.4, and the minimum points were set to 5. Briefly, all scatter dots that fail to form a clear cluster were removed after the treatment. Right: The prediction of events by machine learning. Seven populations, which respectively correspond to D-Lys, D-Arg, D-Phe, D-Tyr, D-Thr, D-Asp, and D-Glu were identified by machine learning. All nanopore measurements were performed as described in Methods. A total of 10 µL acid hydrolysis product was added to *cis* prior to measurement. The event identities (b-c) were predicted by the previously trained machine learning algorithm. The open pore current (I_0) is marked with a dashed line in b.

exceptional biostability.[47–49] Accurate identification of D-peptide components is critical for advancing potential drug candidates.[50] Although direct nanopore sequencing of D-peptides remains unachieved, leveraging the high-resolution capabilities of MspA-NTA-Ni, direct analysis of D-amino acid compositions in D-peptides could, in principle, be demonstrated in this study instead.

A synthetic D-peptide, D-(FREDYTK), composed exclusively of D-amino acids, was custom-synthesized and employed as a model compound for this demonstration (Figure 3a). The peptide underwent acid hydrolysis using 6 M HCl at 110 °C for 20 h[51] to ensure complete cleavage (Methods). The hydrolysate was then neutralized with KOH, lyophilized, and reconstituted in 1 mL of ultra-pure water for subsequent nanopore analysis. For the measurement setup, 10 µL of the prepared solution was added to the *cis* chamber. The raw current trace obtained under these conditions is shown in Figure 3b, revealing distinct event signatures corresponding to different D-amino acids. Continuous data acquisition was performed for 60 min. All recorded events were processed to generate an event scatter plot (Figure 3c, left). To mitigate non-clustered background noise, a DBSCAN (Density-Based Spatial Clustering of Applications with Noise) algorithm was applied (Methods).

Following DBSCAN clustering (Figure 3c, middle) and supervised machine learning classification (Figure 3c, right), seven discrete event clusters were identified, corresponding to D-Phe (F), D-Arg (R), D-Glu (E), D-Asp (D), D-Tyr (Y), D-Thr (T), and D-Lys (K). Quadratic SVM under an error-correcting output codes (ECOC) framework, implemented in MATLAB, performs the classification (Methods). These results are in full agreement with the expected amino acid composition of the parent D-peptide, confirming the reliability of this method for D-peptide composition analysis. By-products of acid hydrolysis of D-peptide were not experimentally observed, most likely due to their inability to interact with MspA-NTA-Ni (Figure S34).

To further evaluate the utility of this nanopore system for D-peptide compositional analysis, acid hydrolysis kinetics of D-(FREDYTK) at multiple time points (4, 8, 14, and 20 h) were measured. The composition and abundance of hydrolyzed D-amino acids at each time point were analyzed using the trained machine learning model. As expected, the proportion of detected D-amino acids progressively increased with hydrolysis time (Figure S35). Additionally, other D-peptides with distinct compositions were tested to demonstrate the method's generality (Figure S36).

Chiral Discrimination of Amino Acids

In nature, amino acids exist primarily as levorotatory (L) enantiomers instead of their dextrorotatory (D) counterparts.[52] Metabolic and enzymatic processes exhibit exquisite stereoselectivity,[53,54] leading to distinct biological activities and toxicological profiles between enantiomers despite their similar physicochemical properties.[50] Synthetic mirror-image proteins[55,56] or naturally occurring peptides,[57,58] composed of arbitrary sequences of all amino acid enantiomers, demand simultaneous enantiomeric discrimination by nanopore as a prerequisite technology for developing corresponding sequencing methods.

Building upon above findings, we expanded our database to include all 39 amino acid enantiomers (Figures 4a,b) to evaluate the discriminatory capacity of MspA-NTA-Ni. Notably, glycine was excluded due to its achirality. Representative ionic current events of enantiomer pairs are visualized in Figure 4b for direct comparison (Video S1). The signal-to-noise ratio (SNR) across multiple nanopore recordings was also evaluated to assess signal clarity and detection robustness (Table S13). The t-distributed stochastic neighbor embedding (t-SNE) algorithm was applied to reduce the dimensionality from 9 to 2, enabling 2D visualization of event distributions (Figure 4c). Although partial overlaps persisted in the ΔI versus SD feature space (Figure S37 and Table S14), simultaneous analysis of all 9 parameters via a supervised machine learning pipeline achieved 98.9% overall accuracy for all 39 amino acids (Table S16). In contrast, however, a 5-dimensional feature space yielded only 96.7% accuracy (Table S15). A comparison is also shown in Figure S38, and the FPR is also summarized in Table S17. By splitting the datasets differently and testing with both five- or nine-feature models in the paired-sample *t*-test (Figure S39), a significant difference between five-feature model and the nine-feature model ($p < 0.0001$) was observed, further confirming the significance of the further included frequency domain parameters.

The quadratic SVM model's confusion matrix (Figure 4d) demonstrated robust discrimination across all enantiomer pairs. A zoomed-in confusion matrix is shown in Figure S40, clearly demonstrating the misclassification patterns. Simultaneous sensing of 20 representative chiral amino acids, including enantiomers of Phe, Trp, Asp, Ile, Lys, Leu, Asn, Ser, Thr, and Tyr was also performed using MspA-NTA-Ni. Considering the differing capture rates of amino acid enantiomers (Table S18), the concentrations of specific analytes were adjusted during mixed sensing to achieve balanced event appearance rates. A representative trace is also shown in Figure 4e, and all events were automatically predicted by machine learning (Figures 4e and S41, S42). Simultaneous sensing of amino acid enantiomers with similar structural features has also been demonstrated (Figures S43, S44). This methodology paves the way for direct enantiomeric profiling in complex matrices such as fermented foods[59] and food additives,[60] offering a high-resolution tool for quality control and safety assessment.

To demonstrate the discrimination of D- and L-amino acids directly from the hydrolysate of a corresponding enantiomeric D- and L-peptide mixture, L-(FREDYTK) and D-(FREDYTK) mixture were hydrolyzed and sensed by MspA-NTA-Ni (Figure S45). The analytical capability of MspA-NTA-Ni for compositional analysis of mixed-chirality peptides was validated by analyzing the hydrolysis products of the chiral peptide Y(DA)GF(DL)[61] (Figure S46).

To further elucidate the chiral recognition mechanism of MspA-NTA-Ni, all-atom molecular dynamics (MD) simulations were performed (Methods), using D/L-Phe as representative analytes (Figures S47–S49). Owing to the configurational disparities between D-Phe and L-Phe upon binding to NTA–Ni, distinct binding modes within the pore lumen were observed in MD simulations, which are a manifestation of chiral discrimination and correlate with their different nanopore event features. While demonstrated with representative analytes, these findings provide valuable insight for understanding the underlying molecular mechanism of chiral discrimination of amino acid enantiomers by MspA-NTA-Ni.

Conclusion

MspA-NTA-Ni analysis of 20 proteinogenic L-amino acids and their D-enantiomers revealed distinct event signatures uniquely associated with each enantiomer, enabling direct identification without prior separation. By incorporating 9 complementary event features, the system achieved a 99.5% validation accuracy for the 19 D-amino acids and glycine. Simultaneous analysis of all 39 amino acid enantiomers yielded an overall accuracy of 98.9%, a significant improvement attributed to the inclusion of frequency-domain features. This methodology was validated through direct sensing of complex D-amino acid mixtures and acid-hydrolyzed

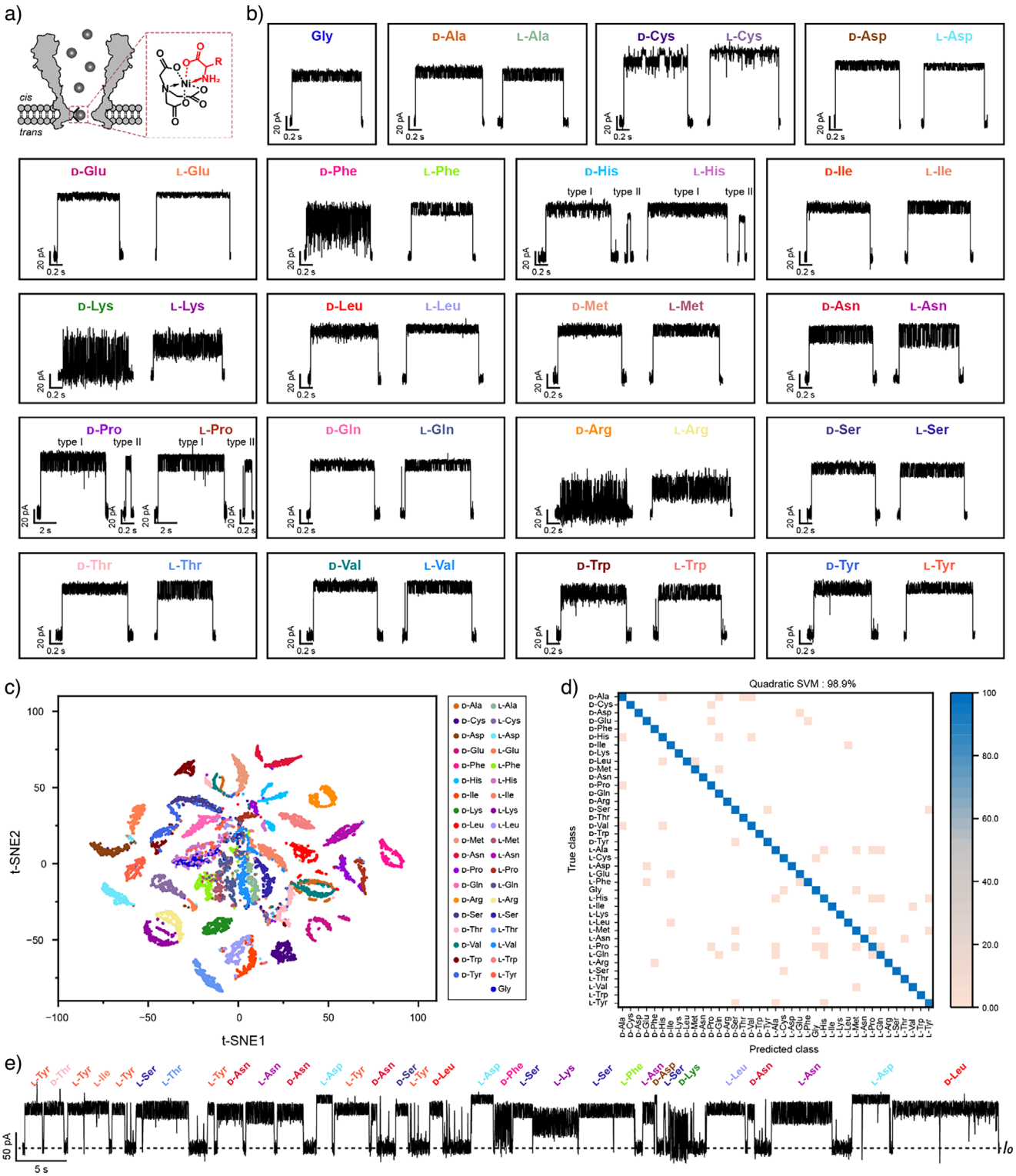

Figure 4. Discrimination between D- and L-amino acids. a) The schematics of amino acid enantiomer sensing when measured with MspA-NTA-Ni. b) Representative amino acid events acquired with MspA-NTA-Ni. Here, the results of 19 pairs of chiral amino acids and glycine are demonstrated in pairs. Discrimination between D- and L-amino acids are clearly demonstrated. c) t-SNE plot generated by dimension reduction of 9 features to a 2D visualization space, representing the 39 amino acid datasets (n=11 700). d) The confusion matrix heatmap of results of 39 amino acids (Figure S40) generated by the quadratic SVM model using the nine-feature machine learning. A validation accuracy of 98.9% is reported (Table S16). e) A representative trace acquired during simultaneous sensing of 20 chiral amino acids. The measurements were performed as described in Methods. A bias of + 100 mV was continually applied. All chiral amino acids were simultaneously added to *cis*. The final concentration of (D, L)-Phe and (D, L)-Trp was 0.1 mM. The final concentration of (D, L)-Asp, (D, L)-Ile, (D, L)-Lys, (D, L)-Leu, (D, L)-Asn, (D, L)-Ser, (D, L)-Thr and (D, L)-Tyr was 0.5 mM. A zoomed-in view of this trace and other raw traces are shown in Figures S41, S42 to show more event details.

D-peptide products, where compositional information was immediately resolved. Manual calculations of separation factors and mahalanobis distances were also performed (Table S19), and the correlations among the features were also evaluated (Figure S50). Some frequency-domain features correlate with time-domain parameters (Figure S50) but still provide complementary, non-redundant contributions (Table S7) to model training. Unlike conventional resistive pulse-based nanopore sensing for biomacromolecules, this study employs a hetero-octameric MspA pore assembly equipped with a single reactive adapter in a chiral sensing environment, thereby achieving full chiral discrimination of all proteinogenic amino acids. Beyond establishing a high-resolution sensor for DL-amino acid analysis, this technology provides a critical enabling component for nanopore exo-sequencing[39] of mirror-image proteins in future prospects.

Supporting Information

The authors have cited additional references within the Supporting Information.[24,36,37,51,62–75]

Acknowledgements

This project was funded by National Key R&D Program of China (Grant No. 2022YFA1304602), National Natural Science Foundation of China (Grant No. 22225405), the Fundamental Research Funds for the Central Universities (Grant No. 020514380336), State Key Laboratory of Analytical Chemistry for Life Science (Grant No. 5431ZZXM2509), National Natural Science Foundation of China (Grant No. 223B2402, to K.F.W), China National Postdoctoral Program for Innovative Talents (Grant No. BX20250087, to K.F.W), Jiangsu Funding Program for Excellent Postdoctoral Talent (Grant No. 2025ZB212, to K.F.W).

The authors also thank the support of High Performance Computing Center of Nanjing University.

Conflict of Interests

The authors declare no conflict of interest.

Data Availability Statement

The data that support the findings of this study are available from the corresponding author upon reasonable request.

Keywords: Amino acid enantiomers · Chiral discrimination · Nanopore · Single-molecule

[1] S. F. Mason, *Nature* **1984**, *311*, 19–23, https://doi.org/10.1038/311019a010.1038/311019a0.
[2] S. Martínez-Rodríguez, A. I. Martínez-Gómez, F. Rodríguez-Vico, J. M. Clemente-Jiménez, F. J. L. Heras-Vázquez, *Chem. Biodiversity* **2010**, *7*, 1531–1548, https://doi.org/10.1002/cbdv.20090024510.1002/cbdv.200900245.
[3] Y. Nagata, T. Fujiwara, K. Kawaguchi-Nagata, Y. Fukumori, T. Yamanaka, *Biochim. Biophys. Acta, Gen. Subj.* **1998**, *1379*, 76–82, https://doi.org/10.1016/S0304-4165(97)00084-6.
[4] J. van Heijenoort, *Nat. Prod. Rep.* **2001**, *18*, 503–519, https://doi.org/10.1039/a804532a10.1039/a804532a.
[5] B. M. Burkhart, D. A. Langs, W. A. Pangborn, W. L. Duax, V. Pletnev, R. M. Gassman, *Biopolymers* **1999**, *51*, 129–144, https://doi.org/10.1002/(SICI)1097-0282(1999)51:2%3c129::AID-BIP3%3e3.0.CO;2-Y10.1002/(SICI)1097-0282(1999)51:2%3c129::AID-BIP3%3e3.0.CO;2-Y.
[6] J. E. Martin, J. Casqueiro, K. Kosalková, A. T. Marcos, S. Gutiérrez, *Antonie Van Leeuwenhoek* **1999**, *75*, 21–31, https://doi.org/10.1023/A:1001820109140.
[7] A. Hashimoto, T. Nishikawa, T. Hayashi, N. Fujii, K. Harada, T. Oka, K. Takahashi, *FEBS Lett.* **1992**, *296*, 33–36, https://doi.org/10.1016/0014-5793(92)80397-Y10.1016/0014-5793(92)80397-Y.
[8] D. S. Dunlop, A. Neidle, D. Mchale, D. M. Dunlop, A. Lajtha, *Biochem. Biophys. Res. Commun.* **1986**, *141*, 27–32, https://doi.org/10.1016/S0006-291X(86)80329-110.1016/S0006-291X(86)80329-1.
[9] C. L. Hao, *Molecules* **2024**, *29*, 1106, https://doi.org/10.3390/molecules2905110610.3390/molecules29051106.
[10] B. H. Fu, Y. W. Liu, J. A. Wang, Z. H. Zhang, X. J. Hu, *Chem. Eng. J.* **2024**, *492*, 152229, https://doi.org/10.1016/j.cej.2024.15222910.1016/j.cej.2024.152229.
[11] L. Pu, *Angew. Chem. Int. Ed. Engl.* **2020**, *59*, 21814–21828, https://doi.org/10.1002/anie.20200396910.1002/anie.202003969.
[12] Y. Cui, Z. Jiang, J. Y. Sun, J. Yu, M. H. Li, M. J. Li, M. X. Liu, X. J. Guo, *Food Chem.* **2014**, *158*, 401–407, https://doi.org/10.1016/j.foodchem.2014.02.13310.1016/j.foodchem.2014.02.133.
[13] Y. C. Sun, T. M. Blattmann, Y. Takano, N. O. Ogawa, Y. Isaji, N. F. Ishikawa, N. Ohkouchi, *Anal. Chem.* **2024**, *96*, 18664–18671, https://doi.org/10.1021/acs.analchem.4c0285110.1021/acs.analchem.4c02851.
[14] N. Florini, F. Faglioni, C. Zucchi, L. Caglioti, G. Pályi, *Amino Acids* **2010**, *38*, 1343–1350, https://doi.org/10.1007/s00726-009-0341-910.1007/s00726-009-0341-9.
[15] M. Claeys-Bruno, D. Toronto, J. Pécaut, M. Bardet, J. C. Marchon, *J. Am. Chem. Soc.* **2001**, *123*, 11067–11068, https://doi.org/10.1021/ja016494x.
[16] F. Kitagawa, K. Otsuka, *J. Chromatogr. B* **2011**, *879*, 3078–3095, https://doi.org/10.1016/j.jchromb.2011.03.01610.1016/j.jchromb.2011.03.016.
[17] C. Simmler, J. G. Napolitano, J. B. McAlpine, S.-N. Chen, G. F. Pauli, *Curr. Opin. Biotechnol.* **2014**, *25*, 51–59, https://doi.org/10.1016/j.copbio.2013.08.00410.1016/j.copbio.2013.08.004.
[18] E. A. Manrao, I. M. Derrington, A. H. Laszlo, K. W. Langford, M. K. Hopper, N. Gillgren, M. Pavlenok, M. Niederweis, J. H. Gundlach, *Nat. Biotechnol.* **2012**, *30*, 349–353, https://doi.org/10.1038/nbt.217110.1038/nbt.2171.
[19] I. M. Derrington, T. Z. Butler, M. D. Collins, E. Manrao, M. Pavlenok, M. Niederweis, J. H. Gundlach, *Proc. Natl. Acad. Sci. USA* **2010**, *107*, 16060–16065, https://doi.org/10.1073/pnas.1001831107.
[20] J. Y. Zhang, S. H. Yan, L. Chang, W. M. Guo, Y. Q. Wang, Y. Wang, P. K. Zhang, H. Y. Chen, S. Huang, *iScience* **2020**, *23*, 100916, https://doi.org/10.1016/j.isci.2020.100916.
[21] H. Ouldali, K. Sarthak, T. Ensslen, F. Piguet, P. Manivet, J. Pelta, J. C. Behrends, A. Aksimentiev, A. Oukhaled, *Nat. Biotechnol.* **2020**, *38*, 176–181, https://doi.org/10.1038/s41587-019-0345-210.1038/s41587-019-0345-2.
[22] S. H. Yan, J. Y. Zhang, Y. Wang, W. M. Guo, S. Y. Zhang, Y. Liu, J. Cao, Y. Q. Wang, L. Y. Wang, F. B. Ma, P. K. Zhang, H. Y. Chen, S. Huang, *Nano Lett.* **2021**, *21*, 6703–6710, https://doi.org/10.1021/acs.nanolett.1c0237110.1021/acs.nanolett.1c02371.

[23] H. Brinkerhoff, A. S. W. Kang, J. Q. Liu, A. Aksimentiev, C. Dekker, *Science* **2021**, *374*, 1509–1513, https://doi.org/10.1126/science.abl438110.1126/science.abl4381.
[24] K. F. Wang, S. Y. Zhang, X. Zhou, X. Yang, X. Y. Li, Y. Q. Wang, P. P. Fan, Y. Q. Xiao, W. Sun, P. K. Zhang, W. F. Li, S. Huang, *Nat. Methods* **2024**, *21*, 92–101, https://doi.org/10.1038/s41592-023-02021-810.1038/s41592-023-02021-8.
[25] Y. Zhang, Y. K. Yi, Z. Y. Li, K. Zhou, L. Liu, H. C. Wu, *Nat. Methods* **2024**, *21*, 102–109, https://doi.org/10.1038/s41592-023-02095-410.1038/s41592-023-02095-4.
[26] K. Motone, D. Kontogiorgos-Heintz, J. Wee, K. Kurihara, S. B. Yang, G. Roote, O. E. Fox, Y. S. Fang, M. Queen, M. Tolhurst, N. Cardozo, M. Jain, J. Nivala, *Nature* **2024**, *633*, 662–669, https://doi.org/10.1038/s41586-024-07935-710.1038/s41586-024-07935-7.
[27] F. P. Qin, M. Q. Sheng, R. J. Li, D. X. Liu, M. L. Ren, R. Tian, L. Douadji, D. Q. Wang, Q. Gan, L. Y. Liang, *Chem. Eng. J.* **2024**, *489*, 151006, https://doi.org/10.1016/j.cej.2024.15100610.1016/j.cej.2024.151006.
[28] A. J. Boersma, H. Bayley, *Angew. Chem. Int. Ed. Engl.* **2012**, *51*, 9606–9609, https://doi.org/10.1002/anie.20120568710.1002/anie.201205687.
[29] J. Cao, W. D. Jia, J. Y. Zhang, X. M. Xu, S. H. Yan, Y. Q. Wang, P. K. Zhang, H. Y. Chen, S. Huang, *Nat. Commun.* **2019**, *10*, 5668, https://doi.org/10.1038/s41467-019-13677-210.1038/s41467-019-13677-2.
[30] Y. L. Guo, A. H. Niu, F. F. Jian, Y. Wang, F. J. Yao, Y. F. Wei, L. Tian, X. F. Kang, *Analyst* **2017**, *142*, 1048–1053, https://doi.org/10.1039/C7AN00097A10.1039/C7AN00097A.
[31] M. Zhang, C. Tang, Z. C. Wang, S. C. Chen, D. Zhang, K. J. Li, K. Sun, C. J. Zhao, Y. Wang, M. Y. Xu, L. Z. Dai, G. W. Lu, H. B. Shi, H. Y. Ren, L. Chen, J. Geng, *Nat. Methods* **2024**, *21*, 609–618, https://doi.org/10.1038/s41592-024-02208-710.1038/s41592-024-02208-7.
[32] L. Ratinho, L. Bacri, B. Thiebot, B. Cressiot, J. Pelta, *ACS Cent. Sci.* **2024**, *10*, 1167–1178, https://doi.org/10.1021/acscentsci.4c0002010.1021/acscentsci.4c00020.
[33] I. Schiopu, S. Iftemi, T. Luchian, *Langmuir* **2015**, *31*, 387–396, https://doi.org/10.1021/la504243r.
[34] J. J. Wang, J. D. Prajapati, F. Gao, Y. L. Ying, U. Kleinekathoefer, M. Winterhalter, Y. T. Long, *J. Am. Chem. Soc.* **2022**, *144*, 15072–15078, https://doi.org/10.1021/jacs.2c0392310.1021/jacs.2c03923.
[35] R. C. A. Versloot, P. Arias-Orozco, M. J. Tadema, F. L. R. Lucas, X. H. Zhao, S. J. Marrink, O. P. Kuipers, G. Maglia, *J. Am. Chem. Soc.* **2023**, *145*, 18355–18365, https://doi.org/10.1021/jacs.3c04076.
[36] S. Y. Zhang, Z. Y. Cao, P. P. Fan, Y. Q. Wang, W. D. Jia, L. Y. Wang, K. F. Wang, Y. Liu, X. Y. Du, C. Z. Hu, P. K. Zhang, H. Y. Chen, S. Huang, *Angew. Chem. Int. Ed. Engl.* **2022**, *61*, e202203769, https://doi.org/10.1002/anie.20220376910.1002/anie.202203769.
[37] Y. Q. Wang, S. Y. Zhang, W. D. Jia, P. P. Fan, L. Y. Wang, X. Y. Li, J. L. Chen, Z. Y. Cao, X. Y. Du, Y. Liu, K. F. Wang, C. Z. Hu, J. Y. Zhang, J. Hu, P. K. Zhang, H. Y. Chen, S. Huang, *Nat. Nanotechnol.* **2022**, *17*, 976–983, https://doi.org/10.1038/s41565-022-01169-2.
[38] T. Z. Butler, M. Pavlenok, I. M. Derrington, M. Niederweis, J. H. Gundlach, *Proc. Natl. Acad. Sci. USA* **2008**, *105*, 20647–20652, https://doi.org/10.1073/pnas.080751410610.1073/pnas.0807514106.
[39] A. Bonini, A. Sauciuc, G. Maglia, *Nat. Methods* **2024**, *21*, 16–17, https://doi.org/10.1038/s41592-023-02136-y10.1038/s41592-023-02136-y.
[40] I. Kiseleva, D. Pyreu, T. Krivonogikh, M. Bazanova, T. Hochenkova, E. Kozlovskii, *Polyhedron* **2013**, *51*, 10–17, https://doi.org/10.1016/j.poly.2012.12.010.
[41] A. Almeida, E. Schubert, J. Smith, J. Wolfe, *Attention Perception & Psychophysics* **2017**, *79*, 1892–1896, https://doi.org/10.3758/s13414-017-1394-610.3758/s13414-017-1394-6.
[42] R. E. Challis, R. I. Kitney, *Med. Biol. Eng. Comput.* **1991**, *29*, 1–17, https://doi.org/10.1007/BF0244629010.1007/BF02446290.
[43] Y. F. Zheng, X. Y. Zhu, M. Y. Jiang, F. F. Cao, Q. You, X. Y. Chen, *Angew. Chem. Int. Ed. Engl.* **2024**, *63*, e202319400, https://doi.org/10.1002/anie.20231940010.1002/anie.202319400.
[44] J. M. Fura, M. J. Sabulski, M. M. Pires, *ACS Chem. Biol.* **2014**, *9*, 1480–1489, https://doi.org/10.1021/cb500268510.1021/cb5002685.
[45] G. Kreil, *Annu. Rev. Biochem.* **1997**, *66*, 337–345, https://doi.org/10.1146/annurev.biochem.66.1.33710.1146/annurev.biochem.66.1.337.
[46] R. B. Merrifield, *J. Am. Chem. Soc.* **1963**, *85*, 2149–2154, https://doi.org/10.1021/ja00897a02510.1021/ja00897a025.
[47] S. B. H. Kent, *Protein Sci.* **2019**, *28*, 313–328, https://doi.org/10.1002/pro.353310.1002/pro.3533.
[48] R. C. D. Milton, S. C. F. Milton, S. B. H. Kent, *Science* **1992**, *256*, 1445–1448, https://doi.org/10.1126/science.160432010.1126/science.1604320.
[49] K. Harrison, A. S. Mackay, L. Kambanis, J. W. C. Maxwell, R. J. Payne, *Nat. Rev. Chem.* **2023**, *7*, 383–404, https://doi.org/10.1038/s41570-023-00493-y10.1038/s41570-023-00493-y.
[50] H. Lorenz, A. Seidel-Morgenstern, *Angew. Chem. Int. Ed. Engl.* **2014**, *53*, 1218–1250, https://doi.org/10.1002/anie.20130282310.1002/anie.201302823.
[51] T. Miyamoto, M. Sekine, T. Ogawa, M. Hidaka, H. Homma, H. Masaki, *J. Pharm. Biomed. Anal.* **2015**, *116*, 105–108. https://doi.org/10.1016/j.jpba.2015.04.022.
[52] M. P. Silverman, J. Badoz, B. Briat, *Opt. Lett.* **1992**, *17*, 886–888, https://doi.org/10.1364/OL.17.00088610.1364/OL.17.000886.
[53] G. A. Strohmeier, H. Pichler, O. May, M. Gruber-Khadjawi, *Chem. Rev.* **2011**, *111*, 4141–4164, https://doi.org/10.1021/cr100386u10.1021/cr100386u.
[54] H. C. S. Chan, L. Pan, Y. Li, S. G. Yuan, *Wiley Interdiscip. Rev.:Comput. Mol. Sci.* **2019**, *9*, e1403.
[55] Y. Xu, T. F. Zhu, *Science* **2022**, *378*, 405–411, https://doi.org/10.1126/science.abm064610.1126/science.abm0646.
[56] G. W. Zhang, T. F. Zhu, *Nat. Chem.* **2024**, *16*, 592–598, https://doi.org/10.1038/s41557-023-01411-x10.1038/s41557-023-01411-x.
[57] Y. Q. Cheng, *ChemBioChem* **2006**, *7*, 471–477, https://doi.org/10.1002/cbic.20050042510.1002/cbic.200500425.
[58] Y. Takada, H. Itoh, A. Paudel, S. Panthee, H. Hamamoto, K. Sekimizu, M. Inoue, *Nat. Commun.* **2020**, *11*. https://doi.org/10.1038/s41467-020-18711-2.
[59] J. Kobayashi, *Microorganisms* **2019**, *7*, 690, https://doi.org/10.3390/microorganisms7120690.
[60] X. Z. Gao, Q. Y. Ma, H. L. Zhu, *Appl. Microbiol. Biotechnol.* **2015**, *99*, 3341–3349, https://doi.org/10.1007/s00253-015-6507-310.1007/s00253-015-6507-3.
[61] M. Staples, S. Acosta, N. Tajiri, M. Pabon, Y. Kaneko, C. V. Borlongan, *Int. J. Mol. Sci.* **2013**, *14*, 17410–17419, https://doi.org/10.3390/ijms14091741010.3390/ijms140917410.
[62] M. J. Abraham, T. Murtola, R. Schulz, S. Páll, J. C. Smith, B. Hess, E. Lindahl, *SoftwareX* **2015**, *1–2*, 19–25, https://doi.org/10.1016/j.softx.2015.06.001.
[63] A. Bernardi, R. Faller, D. Reith, K. N. Kirschner, *SoftwareX* **2019**, *10*, 100241, https://doi.org/10.1016/j.softx.2019.10024110.1016/j.softx.2019.100241.
[64] H. M. A. D. A. Case, K. Belfon, I. Y. Ben-Shalom, S. R. Brozell, D. S. Cerutti, T. E. Cheatham, V. W. D. Cruzeiro III, T. A. Darden, R. E. Duke, G. Giambasu, M. K. Gilson, H.

Gohlke, A. W. Goetz, R. Harris, S. Izadi, S. A. Izmailov, C. Jin, K. Kasavajhala, M. C. Kaymak, E. King, A. Kovalenko, T. Kurtzman, T. S. Lee, S. LeGrand, P. Li, C. Lin, J. Liu, T. Luchko, R. Luo, M. Machado, et al. "Amber 2021", can be found under, **2021** (Accessed 20 May 2025) https://ambermd.org/index.php

[65] T. Darden, D. York, L. Pedersen, *J. Chem. Phys.* **1993**, *98*, 10089–10092, https://doi.org/10.1063/1.46439710.1063/1.464397.

[66] C. J. Dickson, R. C. Walker, I. R. Gould, *J. Chem. Theory Comput.* **2022**, *18*, 1726–1736, https://doi.org/10.1021/acs.jctc.1c0121710.1021/acs.jctc.1c01217.

[67] M. Faller, M. Niederweis, G. E. Schulz, *Science* **2004**, *303*, 1189–1192, https://doi.org/10.1126/science.109411410.1126/science.1094114.

[68] S. Jo, T. Kim, V. G. Iyer, W. Im, *J. Comput. Chem.* **2008**, *29*, 1859–1865, https://doi.org/10.1002/jcc.2094510.1002/jcc.20945.

[69] W. L. Jorgensen, J. Chandrasekhar, J. D. Madura, R. W. Impey, M. L. Klein, *J. Chem. Phys.* **1983**, *79*, 926–935, https://doi.org/10.1063/1.44586910.1063/1.445869.

[70] P. Li, K. M. Merz, Jr., *J. Chem. Theory Comput.* **2014**, *10*, 289–297, https://doi.org/10.1021/ct400751u10.1021/ct400751u.

[71] Z. Li, L. F. Song, P. Li, K. M. Merz, Jr., *J. Chem. Theory Comput.* **2020**, *16*, 4429–4442, https://doi.org/10.1021/acs.jctc.0c0019410.1021/acs.jctc.0c00194.

[72] J. A. Maier, C. Martinez, K. Kasavajhala, L. Wickstrom, K. E. Hauser, C. Simmerling, *J. Chem. Theory Comput.* **2015**, *11*, 3696–3713, https://doi.org/10.1021/acs.jctc.5b0025510.1021/acs.jctc.5b00255.

[73] N. Michaud-Agrawal, E. J. Denning, T. B. Woolf, O. Beckstein, *J. Comput. Chem.* **2011**, *32*, 2319–2327, https://doi.org/10.1002/jcc.2178710.1002/jcc.21787.

[74] A. W. Sousa da Silva, W. F. Vranken, *BMC Res. Notes* **2012**, *5*, 367, https://doi.org/10.1186/1756-0500-5-367.

[75] J. Wang, R. M. Wolf, J. W. Caldwell, P. A. Kollman, D. A. Case, *J. Comput. Chem.* **2004**, *25*, 1157–1174, https://doi.org/10.1002/jcc.20035.

Manuscript received: July 16, 2025
Revised manuscript received: October 05, 2025
Manuscript accepted: October 10, 2025
Version of record online: October 21, 2025